

Using molecular dynamics simulation to study the polarization response of the liquid water interface to surface charge heterogeneity

Sucheol Shin^{a,b} and Adam P. Willard^{a,1}

^aDepartment of Chemistry, Massachusetts Institute of Technology, Cambridge, MA 02139; ^bDepartment of Chemistry, The University of Texas at Austin, Austin, TX 78712

This manuscript was compiled on September 16, 2021

1 The external surfaces of proteins (and other large biomolecules) are chemically and topographically heterogeneous.
2 When a protein is solvated, certain signatures of this heterogeneity are evident in the properties of the surrounding
3 solvent. Understanding how these solvation signatures emerge and what information they convey about protein
4 surface composition is important due to their potential role in facilitating selectivity in small molecule binding or
5 driving recognition in the nascent stages of protein-protein interactions (1–7). The protein surface properties that
6 may be reflected in these signatures, such as charge, hydrophobicity, and local curvature, have differing influences
7 on local water structure and dynamics (8–12). These different influences are mixed and diluted by the correlated
8 fluctuations of water’s interfacial hydrogen bonding network, making their combined effects hard to disentangle or
9 predict. Theory and molecular simulation can be applied to better understand the collective molecular interactions
10 that determine the solvation properties of proteins and other complex surfaces.

11 A significant component of the protein solvation signature originates from electrostatic interactions (1, 5). The
12 charged and polar residues that give rise to these interactions produce a three-dimensional electric field profile
13 that extends into and polarizes the surrounding aqueous environment. Surface charge heterogeneity is reflected in
14 this electric field profile and thereby also in the molecular structure of the liquid water interface. Here, we aim to
15 determine how effectively the fluctuating molecular structure of the adjacent water interface communicates the charge
16 distribution of a surface. We consider the effects of electric field on the orientational statistics of interfacial water
17 molecules and demonstrate how these statistics can be analyzed to quantify water’s polarization response to surface
18 charge heterogeneity. We find that the local polarization response of the water interface is significantly altered by
19 molecular effects that arise due to surface-bound waters. We demonstrate that these molecular effects are sensitive to
20 protein dynamics, highlighting the importance of considering conformational fluctuations when studying hydration
21 properties.

22 Many previous studies have been aimed at understanding the microscopic properties of water at charged and polar
23 surfaces. These properties can be probed with surface sensitive spectroscopies, such as sum-frequency generation
24 spectroscopy (13–15) and terahertz absorption spectroscopy (16, 17), or with dynamic nuclear polarization NMR
25 (8, 18, 19). However, ability to experimentally resolve site-specific details of the solvation environment under room

¹To whom correspondence should be addressed. E-mail: awillard@mit.edu

26 temperature conditions is extremely limited. What experiments have revealed is that strong polar surface–water
27 interactions can significantly modify the hydrogen bonding structure of the liquid water interface and reduce the
28 mobility of interfacial water molecules (20–22). These observations are consistent with the results of simulation
29 studies using both classical (23, 24) and first-principles (25, 26) molecular dynamics (MD) simulation, as well as
30 the predictions of continuum(27, 28) and coarse-grained modeling (29–31). While it is clear that charged and polar
31 surfaces have a significant influence on the properties of their aqueous environments, many of the specific details
32 about water’s interfacial polarization response remain unknown.

33 The polarization response of the liquid water interface involves the realignment of water molecules that are
34 interconnected through strong directional hydrogen bonding interactions. The consequences of these interconnections
35 are not captured by continuum models, such as those based on Poisson-Boltzmann or dielectric continuum theory
36 (32–34), nor are the effects of thermal fluctuations, which introduce significant variation over sub-ns timescales. To
37 study the role that these effects play in protein hydration (and the processes that initiate protein interactions), we
38 utilize all-atom MD, which explicitly describes the collective molecular interactions that govern the aqueous hydrogen
39 bonding network and its response to external electric fields. We demonstrate that molecular-scale details of surface
40 charge can be accurately inferred from only about 20 ps of sampled orientational configurations of interfacial water
41 molecules. However, to make this inference it is necessary to account for both the inherent non-linearity of water’s
42 polarization response, arising from collective hydrogen bonding interactions, and the excluded volume and Coulombic
43 forces arising from surface-bound molecules. We present a computational method that accounts for these effects and
44 show how it can be applied to monitor the influence of protein dynamics on local solvent polarization.

45 In the following section, we consider the influence of a generic uniformly charged surface on the orientational
46 distributions of interfacial water molecules. We highlight that these distributions are not related by simple linear
47 response for biologically relevant surface charge densities. We present a method for analyzing water’s interfacial
48 polarization that accounts for these nonlinearities and demonstrate how the method can be used to infer a surface’s
49 charge distribution. This method is summarized in the subsequent section and described in more detail in the Methods
50 section. By applying this method to a model protein system, we identify how the making and breaking of salt bridges
51 leads to an impulsive change in water’s local polarization profile.

52 **Results and Discussion**

53 **Characterizing polarization response from depth-resolved statistics of interfacial molecular structure.** The molec-
54 ular structure and dynamics of liquid water reflect the strong tendency of molecules to engage in hydrogen bonding.
55 This tendency couples the orientations of adjacent molecules in a way that can influence their response to externally
56 applied electric fields. At an interface, this response is further complicated by the depth-dependent anisotropy of the
57 hydrogen bond network. All-atom MD simulation is an efficient tool for modeling this anisotropy and determining its
58 influence on water’s polarization response.

59 To characterize this influence, we perform simulations of neat liquid water in contact with a model surface that is
60 divided into two oppositely charged regions of tunable surface charge density, $\pm|\sigma_s|$ (Fig. 1A; see Methods section for
61 more detailed description). We analyze these simulations by determining the depth and orientation of each water
62 molecule relative to the plane of the interface. Following Refs. 35 and 9, we specify these quantities in terms of

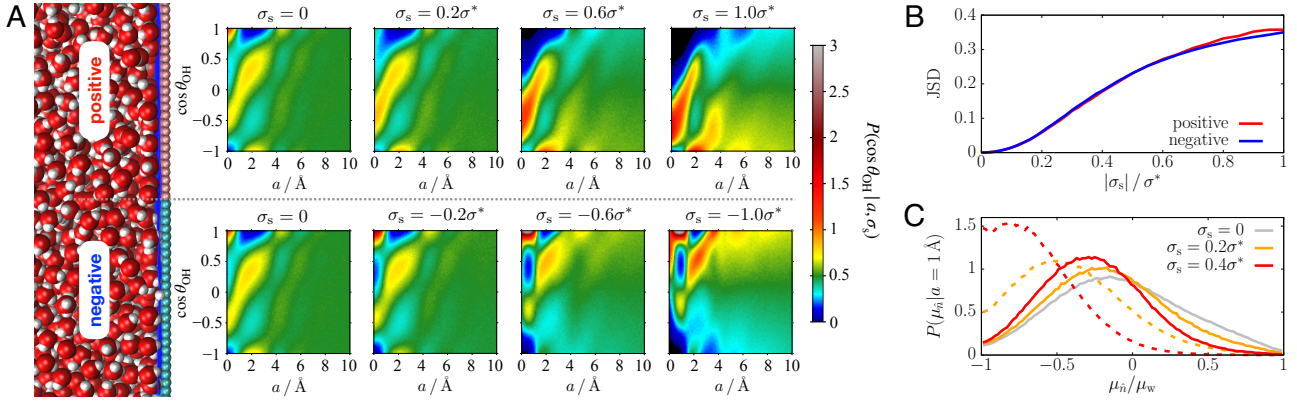


Fig. 1. Effect of surface charge density on the orientational distribution of interfacial water molecules. (A) The left-hand panel contains a simulation snapshot of the charged surface-water interface, where positive and negative surface particles are depicted as pink and cyan spheres, respectively, and the instantaneous liquid water interface is shown in blue. The right-hand panels contain plots of the depth-dependent orientational distribution, $P(\cos \theta_{\text{OH}}|a, \sigma_s)$, for interfacial water molecules at the surfaces with different charge densities, σ_s , where $\sigma^* = 0.85e/\text{nm}^2$. The top and bottom panels show the plots for the surfaces with positive and negative charges, respectively. (B) Plots of JSD [Eq. 4], which compare the distribution of interfacial molecular polarization to the linear response (LR) prediction, are given as a function of σ_s , where the red and blue curves are for $\sigma_s > 0$ and $\sigma_s < 0$ respectively. (C) Comparison of the distribution of the molecular polarization in the surface normal direction, μ_n , at $a = 1 \text{\AA}$ between the simulation (solid line) and LR prediction (dashed line), where μ_w is the dipole moment of a water molecule and the distributions for $\sigma_s = 0, 0.2\sigma^*$, and $0.4\sigma^*$ are shown in gray, orange, and red colors, respectively.

63 $\vec{\kappa} = (\cos \theta_1, \cos \theta_2, a)$, where a denotes the distance of the water molecule from the nearest point of the instantaneous
 64 liquid water interface, and θ_1 and θ_2 are the angles made between each OH bond vector and the local surface
 65 normal. The conditional probability distribution, $P(\vec{\kappa}|\sigma_s)$, encodes the polarization state of a given interface, and the
 66 polarization response can thus be quantified by analyzing how this distribution changes when σ_s is varied.

67 Figure 1A illustrates the sensitivity of interfacial molecular structure to surface charge over a range of positive and
 68 negative surfaces. For ease of visualization, we have projected out one of the angular components of $P(\vec{\kappa}|\sigma_s)$ and
 69 independently normalized the distribution at each value of a to yield the marginal distributions, $P(\cos \theta_1|a, \sigma_s)$. We
 70 observe significant changes in molecular structure with changing surface charge that extend over the first $\sim 1 \text{ nm}$
 71 of the interface. The structure in these distributions reflects the distorted interfacial hydrogen bonding network
 72 (31, 36, 37), and its response to the presence of a uniform electric field. We observe a shift in the peak value of $\cos \theta_1$
 73 for surface molecules (*i.e.*, with $a \leq 3 \text{\AA}$) associated with the alignment of water dipoles with the field, *i.e.*, with
 74 hydrogens pointed toward or away from the negative or positive surface, respectively. The tilt of subsurface molecules
 75 (*i.e.*, with $a \geq 3 \text{\AA}$) with the electric field of the interface is also evident in these distributions.

76 The molecular polarization response of the interface can be quantified by comparing the details of $P(\vec{\kappa}|\sigma_s)$ generated
 77 at differing values of σ_s . If this response is linear, then these distributions can be related by a simple Boltzmann
 78 reweighting that accounts for the coupling of a given $\vec{\kappa}$ to the external electric field. We evaluate the linearity in the
 79 molecular polarization response by assuming that this coupling is given by,

$$80 \quad \epsilon = -\vec{\mu} \cdot \vec{E}, \quad [1]$$

81 where ϵ is the energy of the dipole of a water molecule, $\vec{\mu}$, in a field \vec{E} . The depth-dependent distribution of water
 82 dipoles,

$$83 \quad P(\vec{\mu}|a', \sigma_s) \propto \int \delta(\vec{\mu}_\kappa - \vec{\mu}) \delta(a - a') P(\vec{\kappa}|\sigma_s) d\vec{\kappa}, \quad [2]$$

84 where $\delta(x) = 1$ when $x = 0$ or otherwise equals 0, and $\vec{\mu}_\kappa$ is the value of the dipole vector given by $\vec{\kappa}$, can be predicted
 85 from linear response (LR) as,

$$86 \quad P_{\text{LR}}(\vec{\mu}|a, \sigma_s) \propto P(\vec{\mu}|a, \sigma_s = 0)e^{-\beta\epsilon}, \quad [3]$$

87 where ϵ in this expression uses the field, \vec{E} , associated with the surface charge σ_s . More computational details about
 88 the LR estimation are provided in the [SI Appendix](#).

89 We quantify the accuracy of the LR assumption by computing the Jensen-Shannon divergence,

$$90 \quad \text{JSD} = \frac{1}{2} [\bar{D}_{\text{KL}}(P(\vec{\mu}|a, \sigma_s)||P_{\text{M}}) + \bar{D}_{\text{KL}}(P_{\text{LR}}(\vec{\mu}|a, \sigma_s)||P_{\text{M}})], \quad [4]$$

91 where $P_{\text{M}} = P(\vec{\mu}|a, \sigma_s) + P_{\text{LR}}(\vec{\mu}|a, \sigma_s)$ and \bar{D}_{KL} is the depth-averaged Kullback-Leibler divergence (see the [SI appendix](#)
 92 for more details). This quantity is a metric of the overlap between the LR prediction and the distribution $P(\vec{\mu}|a, \sigma_s)$
 93 sampled directly from MD simulations. Unlike the KL divergence, JSD is symmetric and has an upper bound
 94 ($0 \leq \text{JSD} \leq 1$, if \log_2 is used in evaluating \bar{D}_{KL}). Essentially, $\text{JSD} = 0$ if $P(\vec{\mu}|a, \sigma_s)$ and $P_{\text{LR}}(\vec{\mu}|a, \sigma_s)$ are identical
 95 and $\text{JSD} = 1$ if the distributions have no overlap. For scale, two Gaussian distributions with identical widths and
 96 means separated by their standard deviation yield $\text{JSD} \approx 0.16$. The value of JSD computed across a range of different
 97 surface charge density is plotted in Fig. 1B. We observe that JSD increases rapidly for $|\sigma_s| \lesssim 0.4\sigma^*$ while the increase
 98 rate gets smaller for $|\sigma_s| > 0.4\sigma^*$. Figure 1C illustrates how the distribution of interfacial polarization differs between
 99 the simulation and LR estimate at a given interfacial depth for $\sigma_s = 0.2\sigma^*$ and $0.4\sigma^*$. In each case, the molecular
 100 dipole distribution shift is less than expected based on the LR estimate. The deviation of $P(\vec{\mu}|a, \sigma_s)$ from the LR
 101 estimate indicates that the reorientation of water molecules are significantly affected by the constraints imposed by
 102 the interfacial hydrogen bonding network.

103 **Inferring local surface charge from water’s interfacial molecular structure.** The signatures of water’s nonlinear
 104 response to surface charge are contained within the conditional probability distribution, $P(\vec{\kappa}|\sigma_s)$. If these distributions
 105 are known, then they provide a basis for inferring surface charge from the configurational statistics of interfacial water
 106 molecules. To make this inference, we follow a similar procedure to that of Ref. 9, in which local surface hydrophobicity
 107 is inferred by comparing sampled water configurations to a pre-tabulated distribution, $P(\vec{\kappa}|\text{phob})$, which describes
 108 water’s response to a purely hydrophobic surface. In this subsection, we briefly summarize an approach that adapts
 109 this formalism to the problem of determining local surface charge.

110 To infer surface charge, we employ a strategy based on maximum likelihood estimation (MLE). Specifically, we
 111 sample a set of water configurations adjacent to a surface and compare those configurations to $P(\vec{\kappa}|\sigma_s)$ by computing
 112 the likelihood that those configurations would be spontaneously sampled at a surface with charge density σ_s . We
 113 define the local surface charge estimate, *i.e.*, the apparent surface charge density σ_{MLE} , as the value of σ_s with
 114 the maximum likelihood. By basing the estimate of surface charge on pre-sampled distributions, *i.e.*, $P(\vec{\kappa}|\sigma_s)$, we
 115 implicitly correct for water’s underlying nonlinear response. The specific details of our method are described in
 116 Methods section.

117 **Evaluating how surface charge heterogeneity is reflected in water’s interfacial molecular structure.** Many hydrated
 118 surfaces, including those of proteins, have surface charge heterogeneity over molecular length scales. To assess how

119 heterogeneity on these length scales affects the polarization response of the adjacent liquid water interface, we study a
 120 tunable model surface in contact with a slab of liquid water. Specifically, our model surface comprises an immobilized
 121 snapshot of bulk liquid water molecules at equilibrium as described by the SPC/E force field at $T = 300\text{K}$ and near
 122 conditions of liquid-vapor phase coexistence. The exposed face of this rigid water model surface includes all molecules
 123 whose oxygens reside on one side of a plane drawn through a configuration of a periodically replicated slab of the
 124 bulk liquid. The model surface thus includes a disordered distribution of surface charge, as given by the partial
 125 charges of the immobilized water molecules, that we tune through a uniform scaling by parameter α , such that $\alpha = 0$
 126 corresponds to an uncharged (hydrophobic) surface and $\alpha = 1$ corresponds to the surface with the specific charge
 127 amplitudes of liquid water. More details about the model surface are contained within the [SI Appendix for preparing
 128 this model surface and simulating its aqueous interfacial system](#).

129 To study the influence of the heterogeneous surface on water’s interfacial polarization, we carry out simulations of
 130 a slab of liquid water in contact with model surfaces with a variety of different values of α . For each value of α , we
 131 generate a spatially resolved interfacial polarization map by sampling configurations of interfacial water molecules
 132 located over specific points along the surface and using those sampled configurations to compute the corresponding
 133 value of σ_{MLE} . Figure 2 contains the results of these calculations for the model surface with several different values
 134 of α . We find that the specific pattern of the actual surface charge distribution, σ_s (Fig. 2A; see [SI Appendix for
 135 the details about estimating \$\sigma_s\$](#)), is accurately reflected in the polarization response of water when α is small, *e.g.*,
 136 $\alpha \lesssim 0.4$ (Fig. 2B). However, when α is larger, the map of σ_{MLE} deviates from that of the underlying surface charge
 137 (Fig. 2C), indicating the emergence of lateral correlations in water’s interfacial polarization response.

138 To quantify the correspondence between σ_{MLE} and σ_s , we compare values generated at different points along the
 139 model surface. Figure 2D contains a scatter plot of all possible surface points that illustrates this correspondence. We
 140 observe much better agreement (*i.e.* narrower spread) between σ_{MLE} and σ_s when $\alpha = 0.4$ ($R^2 = 0.86$) than when
 141 $\alpha = 1.0$ ($R^2 = 0.65$), where only the qualitative features of charge heterogeneity are reflected in water’s interfacial
 142 polarization response. We further quantify the correspondence between σ_{MLE} and σ_s by computing the mean unsigned
 143 error (MUE),

$$144 \quad \text{MUE} = \frac{1}{N_{\text{surf}}} \sum_{i=1}^{N_{\text{surf}}} |\sigma_{\text{MLE},i} - \sigma_{s,i}|, \quad [5]$$

145 where the summation is taken over all N_{surf} points sampled along the surface. As Fig. 2E illustrates, we observe a
 146 significant increase in the difference between σ_{MLE} and σ_s for $\alpha \gtrsim 0.4$. This increase signals the onset of non-ideal
 147 response, whereby the local polarization of the interface is significantly influenced by lateral molecular correlations. As
 148 the more discrete structure of the data plotted in Fig. 2C suggests, these lateral correlations arise when surface sites
 149 manage to pin individual water molecules. We provide a quantitative evidence for this interpretation in [SI Appendix,
 150 Fig. S5 by tracking the number of interfacial water molecules and its fluctuations at a given location on the surface](#).

151 **Role of Water–Water Interactions in the Nonlinear Response of Interfacial Water.** When strong surface–water in-
 152 teractions cause water molecules to be fully or partially immobilized at specific surface sites, those bound water
 153 molecules augment the effective surface charge distribution. In a sense, bound water molecules act as a component
 154 of the surface itself. By accounting for the electrostatic influence of surface-bound water molecules, the interfacial

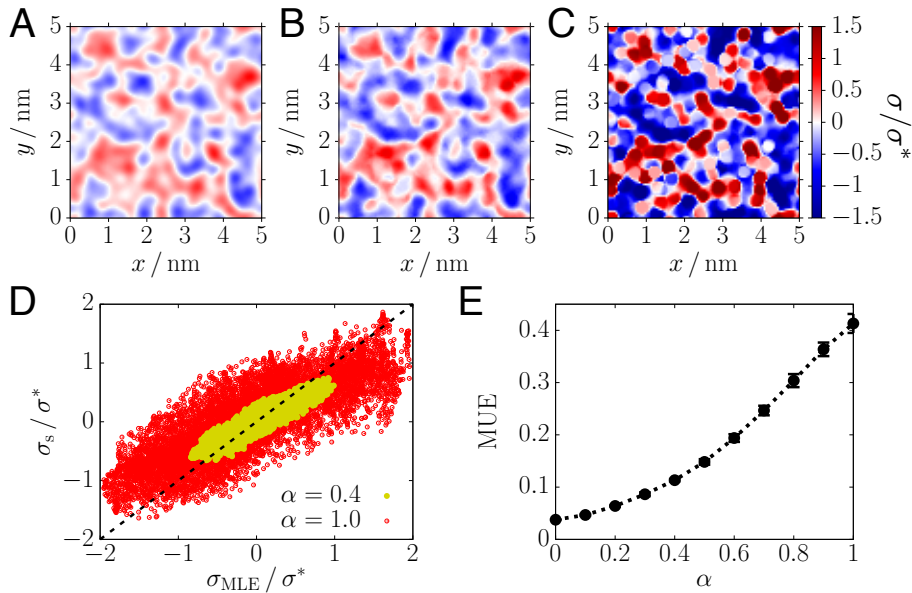


Fig. 2. Surface charge heterogeneity is reflected in water’s interfacial molecular structure. (A) A spatial map of the heterogeneous surface charge density, σ_s , indicated by shading, for $\alpha = 0.4$. (B-C) A spatial map of the inferred surface charge density, σ_{MLE} , indicated by shading, for $\alpha = 0.4$ and $\alpha = 1.0$, respectively. Panels (A-C) share the same color scale. (D) A scatter plot illustrating the correlation between the actual (σ_s) and inferred (σ_{MLE}) values of surface charge density computed at points along the surface with $\alpha = 0.4$ (yellow points) and $\alpha = 1.0$ (red points). Dashed line represents the perfect correlation, $\sigma_s = \sigma_{MLE}$. (E) Plot of the α dependence of the mean unsigned error [Eq. 5]. The dotted line is a guide to the eye.

155 polarization response can be more accurately predicted at larger values of α .

156 To account for the electrostatic influence of other water molecules, we evaluate the electric field at the center of
 157 each water molecule, due to the surrounding solvent. Then, we project this field perpendicular to the interface and
 158 use Gauss’s law to infer an effective local surface charge density, σ_{liq} (see SI Appendix for more details). Using this
 159 effective surface charge, we define a total effective surface charge density,

$$160 \quad \sigma_{tot} = \sigma_s + \sigma_{liq}, \quad [6]$$

161 that combines the influence of the local surface and its impact on the surrounding liquid. The results of this
 162 decomposition are presented in Fig. 3.

163 Figure 3A contains plots of σ_{liq} for various values of α . We observe that σ_{liq} highlights the positions and local
 164 electrostatic influence of pinned water molecules (see also SI Appendix, Fig. S6B). As illustrated in Fig. 3B, the
 165 predicted surface charge, σ_{MLE} , agrees better with the total effective surface charge including σ_{liq} than σ_s alone, with
 166 mean errors of 0.31 ± 0.01 and 0.41 ± 0.02 for $\alpha = 1$, respectively (see SI appendix, Fig. S6C for the comparison
 167 of errors in the full range of α .) These results thus highlight the role of water–water interactions in the non-ideal
 168 response of σ_{MLE} for surfaces with highly polar surface sites, and thus indicate that collective aspects of water’s
 169 interfacial polarization can be accounted for by specifying the average electrostatic state of the local environment.

170 We can gain insight into the role of surrounding waters in determining local polarization response by considering
 171 the relative contributions of σ_s and σ_{liq} to σ_{tot} . Figure 3C contains a plot of the average (over all surface points)
 172 magnitude of the perpendicular electric field arising from the surface itself and the surrounding liquid as a function of
 173 α . We report these quantities in terms of their equivalent surface charges, σ_s and σ_{liq} . We observe a roughly linear

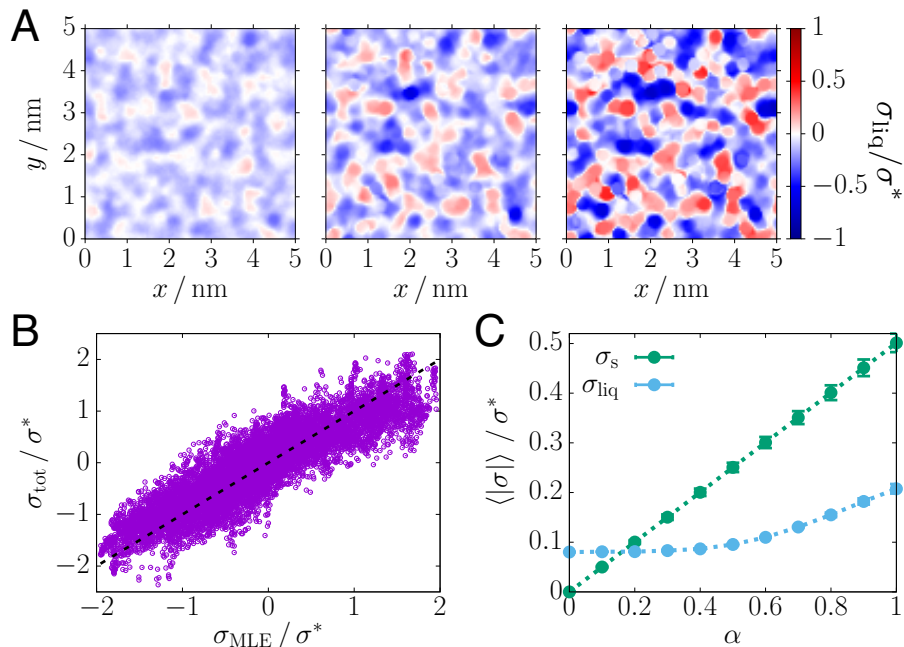


Fig. 3. Role of water–water interactions in the response of water’s interfacial molecular structure to surface charge. (A) Spatial maps of σ_{liq} for the surface analyzed in Fig. 2, with $\alpha = 0.4$ (left), 0.7 (center), and 1 (right). The shading indicates the charge density value in units of σ^* as given in the color bar on the right. (B) Scatter plot between σ_{tot} and σ_{MLE} for $\alpha = 1.0$. The dashed line represents the exact correspondence, $\sigma_{\text{tot}} = \sigma_{\text{MLE}}$. (C) Plots of the α dependence of $\langle |\sigma_s| \rangle$ and $\langle |\sigma_{\text{liq}}| \rangle$, shown in green and sky-blue circles, respectively. The dotted lines are a guide to the eye.

174 increase in the contribution of the surface with α , as expected. However, we find a more complicated trend arising
 175 from the surrounding liquid, whereby σ_{liq} exhibits little change for $0 \leq \alpha \lesssim 0.4$ and a sharp increase for $\alpha \gtrsim 0.4$. This
 176 increase reflects the growing importance of surface-bound water molecules in influencing the polarization response of
 177 their surroundings. Due to this influence, the polarization response of a water interface cannot be reliably predicted
 178 based on the surface charge alone, except for cases where surface polarity is sufficiently uniform or sufficiently small.

179 **Dynamic local polarization at the protein-water interface.** We extend our approach to study protein surfaces, which
 180 are both chemically and topographically heterogeneous as well as dynamic due to the thermal fluctuations of the
 181 backbone and the side chains. By including the influence of equilibrium protein fluctuations, we can assess the role of
 182 conformational dynamics and intra-protein interactions, such as salt bridges, in determining the polarization response
 183 of the surrounding aqueous environment. We illustrate this role in the context of the *Escherichia coli* chemotaxis
 184 signaling protein, CheY (PDB code: 1JBE), which we take as a representative model protein system. The backbone
 185 structure of this 128 residue protein, as illustrated in Fig. 4A, presents 90-100 surface residues in the folded state, 33
 186 of which have charged side chains capable of forming salt bridges.

187 We analyze the aqueous interfacial polarization response by computing σ_s and σ_{MLE} on an array of points along
 188 the protein surface (see SI Appendix for computational details). Figure 4B illustrates how these computed values
 189 relate when the protein structure is fixed in a single folded configuration. We observe that the qualitative features
 190 of the surface charge distribution, such as the location and shape of positively and negatively charged regions, are
 191 captured in σ_{MLE} . This observation implies that water’s local polarization response contains information about the
 192 underlying protein surface charge. However, the point-by-point agreement between σ_s and σ_{MLE} is not quantitative,

193 with a MUE of 0.46, indicating a prevalence of non-local correlations in water’s interfacial polarization response.

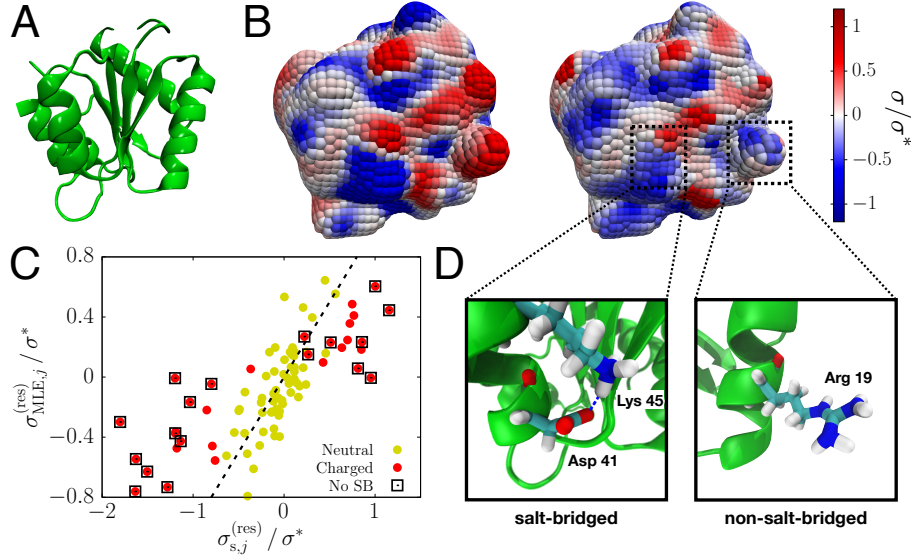


Fig. 4. Water’s interfacial polarization response around a protein. (A) Simulation snapshot of the CheY protein (surrounding water molecules and ions are omitted for clarity) showing its structural backbone. (B) Spatial maps of σ_s (left) and σ_{MLE} (right) computed for points along the protein surface. (C) Scatter plot between $\sigma_{MLE,j}^{(res)}$ and $\sigma_{s,j}^{(res)}$ for each surface residue. We distinguish residues with neutral side chains and charged side chains by yellow and red points, respectively, and we indicate non-salt-bridged (No SB) residues with an additional box around the point. The dashed line corresponds to the perfect correlation, $\sigma_{MLE,j}^{(res)} = \sigma_{s,j}^{(res)}$. (D) An illustration of the differences in side chain alignment for salt-bridged and non-salt-bridged residues.

194 To gain physical insight, we compute the net polarization response of water around each surface residue. Specifically,
 195 we identify the nearest residue of each surface point and then average σ_{MLE} over all points belonging to each individual
 196 residue. So the apparent surface charge density of residue j is defined as,

$$197 \quad \sigma_{MLE,j}^{(res)} = \frac{1}{N_{surf}(j)} \sum_{i \in n(j)} \sigma_{MLE,i}^{(res)}, \quad [7]$$

198 where $n(j)$ is the set of surface points whose nearest residue is j and $N_{surf}(j)$ is the number of these points. We define
 199 $\sigma_{s,j}^{(res)}$ in an analogous way. Figure 4C contains a scatter plot of these calculations, illustrating that the correspondence
 200 between interfacial polarization and local surface charge differs significantly between neutral and charged residues.
 201 Specifically, by comparing the slopes of the linear best fit to each set of points, it appears that σ_{MLE} is systematically
 202 less sensitive to σ_s around charged residues (slope = 0.34) than neutral residues (slope = 0.87). Notably, this relative
 203 insensitivity was not observed for the model surface (Fig. 2).

204 We observe that when charged residues are involved in the formation of salt bridges, they tend to exhibit smaller
 205 differences between $\sigma_{MLE,j}^{(res)}$ and $\sigma_{s,j}^{(res)}$. We hypothesize that the origin of these smaller differences is related to the
 206 geometric arrangements of the side chains which can affect the lateral correlations of nearby interfacial water molecules.
 207 The side chains of typical charged residues can protrude into the surrounding water interface, however, the formation
 208 of a salt bridge tends to flatten side chains’ orientations so that they align parallel to the local protein surface. We
 209 illustrate this orientational difference in Fig. 4D. While flattened side chains present a distinct set of charged groups
 210 on which interfacial water molecules can be pinned, those that protrude into the surrounding liquid contribute to
 211 disrupting local water structure, which is far from the liquid interface, perhaps in the second or third hydration

212 shell. Consequently, the aqueous interfacial polarization near salt-bridged side chains is enhanced whereas the local
 213 hydration environment near non-salt-bridged ones is depolarized in a way that extends beyond simple polarization.

214 The data presented in Fig. 4 was generated for a single fixed configuration of the protein. However, the local
 215 hydration structure of a protein can be quite sensitive to equilibrium protein conformational fluctuations. We
 216 examine the influence of protein dynamics by computing time-resolved values of $\sigma_{\text{MLE},j}^{(\text{res})}$ and $\sigma_{\text{s},j}^{(\text{res})}$. Specifically, we
 217 define $\sigma_{\text{MLE},j}^{(\text{res})}(t)$ and $\sigma_{\text{s},j}^{(\text{res})}(t)$ by analyzing water configurations only within a 20-ps time window from time t (see SI
 218 Appendix for computational details). Figure 5A contains a plot of $\Delta\sigma_j^{(\text{res})}(t) = \sigma_{\text{MLE},j}^{(\text{res})}(t) - \sigma_{\text{s},j}^{(\text{res})}(t)$ for two specific
 219 residues over 10 ns of the simulated protein dynamics with no restraint on the conformation. We find that the
 220 apparent surface charge surrounding the neutral residue, Asn62, does not exhibit a significant difference from the
 221 actual surface charge as $\Delta\sigma_{\text{Asn62}}^{(\text{res})}$ fluctuates steadily around zero. We observe similar behavior for other neutral surface
 222 residues. On the other hand, the time series for $\Delta\sigma_j^{(\text{res})}$ for the charged residue, Glu67, exhibits large fluctuations
 223 that are indicative of two distinct underlying charge states, one at $\Delta\sigma_{\text{Glu67}}^{(\text{res})} \approx 1$ and the other at $\Delta\sigma_{\text{Glu67}}^{(\text{res})} \approx 1.5$.
 224 We attribute these dynamics to the making and breaking of a salt bridge. We support this claim by comparing
 225 the fluctuations of $\Delta\sigma_{\text{Glu67}}^{(\text{res})}$ to the fluctuations in the distance between Glu67 and Lys70, $d_{\text{SB}}(67,70)$, which act as
 226 an intermittent salt bridge pair. We observe that the large changes in $\Delta\sigma_{\text{Glu67}}^{(\text{res})}$ coincide with those of $d_{\text{SB}}(67,70)$,
 227 indicating that salt bridge formation leads to a concomitant increase in the local solvent polarization. We provide
 228 more direct evidences for the relationship between salt bridge formation and local solvent polarization by analyzing
 229 $\sigma_{\text{Glu67}}^{(\text{res})}(t)$ in SI Appendix, Figs. S7A-S7B.

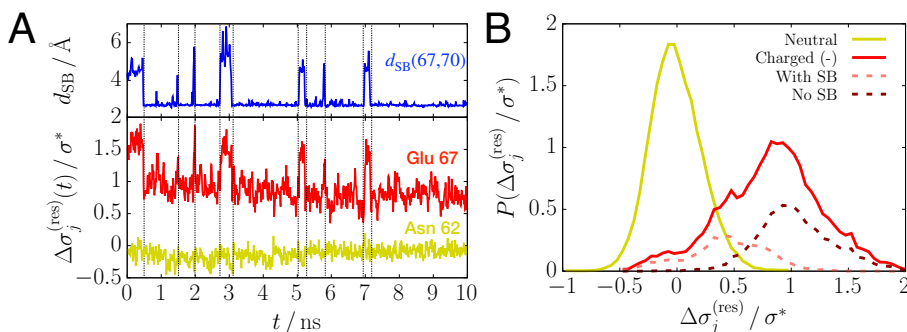


Fig. 5. Water's interfacial molecular structure reveals the dynamic context of nonlocal interactions between the charged residues. (A) Plots of $\Delta\sigma_j^{(\text{res})}(t)$ for two specific residues computed from a 10-ns trajectory of the dynamic protein (red and yellow lines, bottom), where the fluctuations of $\Delta\sigma_{\text{Glu67}}^{(\text{res})}(t)$ are coupled with the salt bridge formation reflected in the distance between Glu67 and the other interacting residue, Lys70 (blue line, top). (B) Plots of probability distribution of $\Delta\sigma_j^{(\text{res})}$, where the distributions for residues with net charge of zero and negative net charge are shown in yellow and red solid lines, respectively. For the negatively charged residues, the distribution is further decomposed into the cases with and without salt bridges (SB), which are shown in light-red and dark-red dashed lines, respectively.

230 We further highlight the distinction between neutral, charged, and salt-bridged residues by computing the probability
 231 distribution of $\Delta\sigma_j^{(\text{res})}$ for each residue population. As illustrated in Fig. 5B, the distribution for neutral residues is
 232 centered around zero, with a relatively narrow distribution (variance = 0.055). In contrast, the distribution of $\Delta\sigma_j^{(\text{res})}$
 233 for negatively charged residues is relative broad (variance = 0.42) and centered at a positive value of $\Delta\sigma^{(\text{res})}$. This
 234 non-zero positive mean implies that the hydration layer around negatively charged residues tends to be less polarized
 235 than one would expect based on the residue charge alone. We find an analogous phenomena for positively charged
 236 residues, *i.e.*, giving rise to a broad distribution centered at negative values of $\Delta\sigma^{(\text{res})}$ (SI Appendix, Fig. S7C).

237 Figure 5B also contains distributions for the subpopulations of salt-bridged and non-salt-bridged negatively charged
 238 residues. Analysis of these subpopulations highlights that salt bridge formation has the effect of systematically
 239 polarizing the local hydration environment. Overall, the results from the dynamic protein further rationalize the
 240 implications from the static case.

241 **Qualitative differences in the polarization response at the model and protein surfaces.** We now remark on notable
 242 similarities and differences between the results generated for our tunable model surface and those generated for
 243 the CheY protein. We only find close correspondence between σ_{MLE} and σ_s in the case where the magnitude of
 244 local surface charge is low, such as when $\alpha \leq 0.4$ or in the vicinity of neutral surface residues. Under these low
 245 charge conditions, *i.e.*, having local Coulomb interactions below approximately 0.59 kcal/mol or $1 k_B T$, the spatial
 246 characteristics of water’s interfacial polarization response will mirror that of the underlying surfaces. However, when
 247 surfaces have charge sites that are strongly attractive to water molecules, the spatial characteristics of the interfacial
 248 polarization response are influenced by lateral correlations. These correlations can be accounted for by resolving the
 249 electric field contributions of the surrounding liquid, but also are affected by the local topography of the surface,
 250 including the effects due to the protrusion of charged side chains into the liquid.

251 Our results highlight the significant influence of protein conformational fluctuations on the polarization response of
 252 the surrounding aqueous interface. Along with thermal fluctuations in the specific relative positions of the charged
 253 surface residues, the formation of salt bridges has a large local effect on interfacial polarization. Specifically, salt bridge
 254 formation contributes to enhancing the effects of the fields that emerge from the side chains that are involved. The
 255 transient dynamics of salt bridge formation and deformation are thus relayed to the surrounding liquid via changes in
 256 water’s interfacial polarization response. These changes may play a role in modulating the water-mediated effects
 257 that drive conformational changes (38–40) or the nascent stages of protein-protein (41) or protein-ligand binding (2).

258 Methods

260 **Maximum likelihood estimation.** We characterize the aqueous interfacial molecular structure of a particular interfacial system
 261 by sampling values of $\vec{\kappa}$ and comparing them to $P(\vec{\kappa}|\text{ref})$, where the reference system is varied systematically in the specific
 262 surface feature. We describe the variation of the reference system using a parameter for the given surface feature, σ (*e.g.*,
 263 surface charge density for this study), such that the probability for observing a particular orientation in the reference system is
 264 also parametrized as $P(\vec{\kappa}|\sigma)$. With this parametrization, we can compare quantitatively the sampled molecular orientations,
 265 $\mathbb{K} = \{\vec{\kappa}_1, \vec{\kappa}_2, \dots, \vec{\kappa}_N\}$, to those from reference interfacial systems for different σ , based on the likelihood function given by

$$266 \quad \mathcal{L}(\sigma|\mathbb{K}) = \prod_{i=1}^N P(\vec{\kappa}_i|\sigma) . \quad [8]$$

267 This quantity represents the probability that the given set of molecular configurations occurs spontaneously in the reference
 268 system having the surface property of σ . $\mathcal{L}(\sigma|\mathbb{K})$ has a larger value when the interfacial molecular structure is closer to that of
 269 the reference system with σ . Therefore, the value of σ that maximizes the likelihood function,

$$270 \quad \sigma_{\text{MLE}} = \arg \max_{\sigma} \mathcal{L}(\sigma|\mathbb{K}) , \quad [9]$$

271 reflects the optimal extent of the given surface property which underlies water’s interfacial molecular structure in the system
 272 of interest. We can also quantify the likelihood function with spatial and temporal resolution by analyzing the molecular

273 configurations sampled at a given surface location, \vec{r}_s , and time, t . Maximizing such a likelihood function will specify $\sigma_{\text{MLE}}(\vec{r}_s, t)$.
274 More details about computing $\sigma_{\text{MLE}}(\vec{r}_s, t)$ and its time average are provided in [SI Appendix](#).

275 **Simulation details.** To obtain the reference orientational distributions, $P(\vec{\kappa}|\sigma_s)$, we simulated a slab of liquid water in contact
276 with a surface of given charge density in the NVT ensemble using the LAMMPS package (42). 2,474 SPC/E water molecules
277 (43) were put into a simulation cell with dimensions $5 \times 5 \times 12 \text{ nm}^3$ measured in x -, y -, and z -directions, respectively. As the
278 simulation cell is long enough in the z -dimension, water molecules spontaneously condense into a slab with a thickness of
279 $\sim 3 \text{ nm}$ at 298 K. To mimic a charged surface, point charges were placed on a square lattice with a 1 \AA lattice constant at the
280 bottom of the simulation cell along with the 9-3 Lennard-Jones (LJ) potential which represents soft repulsive interactions
281 against water (44, 45). The LJ potential between the surface and individual water molecules is given by

$$282 \quad u(r) = \epsilon_{\text{LJ}} \left[\frac{2}{15} \left(\frac{\sigma_{\text{LJ}}}{r} \right)^9 - \left(\frac{\sigma_{\text{LJ}}}{r} \right)^3 \right] + \frac{13}{15} \epsilon_{\text{LJ}}, \quad r < \sigma_{\text{LJ}} \quad [10]$$

283 where r is distance of a water molecule from the surface and the same LJ parameters were used for ϵ_{LJ} and σ_{LJ} as those for
284 SPC/E water, *i.e.*, $\epsilon_{\text{LJ}} = 0.650 \text{ kJ/mol}$ and $\sigma_{\text{LJ}} = 3.166 \text{ \AA}$. One half of the surface (*i.e.*, $x < 25 \text{ \AA}$) has positive charges of
285 q_s and the other half (*i.e.*, $x > 25 \text{ \AA}$) has negative charges of $-q_s$, so the entire system is electrically neutral. The molecular
286 orientations were sampled from the regions of $5 \text{ \AA} < x < 20 \text{ \AA}$ and $30 \text{ \AA} < x < 45 \text{ \AA}$ to represent the statistics for the surfaces
287 with charge densities, $\sigma_s = q_s/\text{\AA}^2$, and $\sigma_s = -q_s/\text{\AA}^2$, respectively. The simulation cell was periodically replicated along x - y
288 directions, and the long-range part of electrostatic interactions were computed by the two-dimensional Particle Mesh Ewald
289 method with a cutoff distance of 10 \AA (46). Molecular geometries of water were constrained by the SHAKE algorithm (47).
290 Propagation of dynamics was based on the standard velocity-Verlet integrator with a time step of 2 fs. Water molecules were
291 coupled to the Langevin thermal bath at $T = 298 \text{ K}$. The system was equilibrated for 0.1 ns prior to the production run of 2 ns
292 along which a simulation snapshot was taken every 0.1 ps. For a surface of given charge density, statistics were collected from
293 six independent trajectories.

294 **ACKNOWLEDGMENTS.** We acknowledge useful discussions with Professors Songi Han, Liang Shi, and Rick Remsing.
295 This work was supported by the National Science Foundation under CHE-1654415 and also partially (SS) by the Kwanjeong
296 Educational Foundation in Korea.

- 297 1. Ball P (2008) Water as an active constituent in cell biology. *Chemical Reviews* 108(1):74–108.
- 298 2. Chung E, et al. (1998) Mass spectrometric and thermodynamic studies reveal the role of water molecules in complexes formed between SH2 domains and tyrosyl phosphopeptides. *Structure*
299 6(9):1141–1151.
- 300 3. Papoian GA, Ulander J, Wolynes PG (2003) Role of water mediated interactions in protein-protein recognition landscapes. *Journal of the American Chemical Society* 125(30):9170–9178.
- 301 4. Fernández A, Scheraga HA (2003) Insufficiently dehydrated hydrogen bonds as determinants of protein interactions. *Proceedings of the National Academy of Sciences of the United States of*
302 *America* 100(1):113–118.
- 303 5. Levy Y, Onuchic JN (2006) Water Mediation in Protein Folding and Molecular Recognition. *Annual Review of Biophysics and Biomolecular Structure* 35(1):389–415.
- 304 6. Beuming T, et al. (2012) Thermodynamic analysis of water molecules at the surface of proteins and applications to binding site prediction and characterization. *Proteins: Structure, Function and*
305 *Bioinformatics* 80(3):871–883.
- 306 7. Pan AC, et al. (2019) Atomic-level characterization of protein–protein association. *Proceedings of the National Academy of Sciences of the United States of America* 116(10):4244–4249.
- 307 8. Barnes R, et al. (2017) Spatially Heterogeneous Surface Water Diffusivity around Structured Protein Surfaces at Equilibrium. *Journal of the American Chemical Society* 139(49):17890–17901.
- 308 9. Shin S, Willard AP (2018) Characterizing Hydration Properties Based on the Orientational Structure of Interfacial Water Molecules. *Journal of Chemical Theory and Computation* 14(2):461–465.
- 309 10. Weiß RG, Heyden M, Dzubiella J (2015) Curvature Dependence of Hydrophobic Hydration Dynamics. *Physical Review Letters* 114(18):19–21.
- 310 11. Rego NB, Xi E, Patel AJ (2019) Protein Hydration Waters Are Susceptible to Unfavorable Perturbations. *Journal of the American Chemical Society* 141(5):2080–2086.
- 311 12. Heyden M (2019) Heterogeneity of water structure and dynamics at the protein-water interface. *Journal of Chemical Physics* 150(9):094701.
- 312 13. Shultz MJ, Schnitzer C, Simonelli D, Baldelli S (2000) Sum frequency generation spectroscopy of the aqueous interface: Ionic and soluble molecular solutions. *International Reviews in Physical*
313 *Chemistry* 19(1):123–153.
- 314 14. Richmond GL (2002) Molecular bonding and interactions at aqueous surfaces as probed by vibrational sum frequency spectroscopy. *Chemical Reviews* 102(8):2693–2724.

- 315 15. Shen YR, Ostroverkhov V (2006) Sum-Frequency Vibrational Spectroscopy on Water Interfaces: Polar Orientation of Water Molecules at Interfaces. *Chemical Reviews* 106(4):1140–1154.
- 316 16. Ebbinghaus S, et al. (2007) An extended dynamical hydration shell around proteins. *Proceedings of the National Academy of Sciences of the United States of America* 104(52):20749–20752.
- 317 17. Heyden M, et al. (2008) Long-range influence of carbohydrates on the solvation dynamics of water-answers from terahertz absorption measurements and molecular modeling simulations. *Journal*
318 *of the American Chemical Society* 130(17):5773–5779.
- 319 18. McCarney ER, Armstrong BD, Kausik R, Han S (2008) Dynamic nuclear polarization enhanced nuclear magnetic resonance and electron spin resonance studies of hydration and local water
320 dynamics in micelle and vesicle assemblies. *Langmuir* 24(18):10062–10072.
- 321 19. Armstrong BD, Han S (2009) Overhauser dynamic nuclear polarization to study local water dynamics. *J. Am. Chem. Soc.* 131(13):4641–4647.
- 322 20. Heugen U, et al. (2006) Solute-induced retardation of water dynamics probed directly by terahertz spectroscopy. *Proceedings of the National Academy of Sciences* 103(33):12301–12306.
- 323 21. Armstrong BD, et al. (2011) Site-specific hydration dynamics in the nonpolar core of a molten globule by dynamic nuclear polarization of water. *Journal of the American Chemical Society*
324 133(15):5987–5995.
- 325 22. Wen YC, et al. (2016) Unveiling Microscopic Structures of Charged Water Interfaces by Surface-Specific Vibrational Spectroscopy. *Physical Review Letters* 116(1):016101.
- 326 23. Giovambattista N, Debenedetti PG, Rossky PJ (2007) Effect of surface polarity on water contact angle and interfacial hydration structure. *Journal of Physical Chemistry B* 111(32):9581–9587.
- 327 24. Conti Nibali V, Havenith M (2014) New insights into the role of water in biological function: Terahertz absorption spectroscopy and molecular dynamics simulations studies of the solvation dynamics
328 of biomolecules. *J. Am. Chem. Soc.* 136:12800–12807.
- 329 25. Heyden M, et al. (2010) Dissecting the THz spectrum of liquid water from first principles via correlations in time and space. *Proceedings of the National Academy of Sciences of the United States*
330 *of America* 107(27):12068–12073.
- 331 26. Gaigeot MP, Sprik M, Sulpizi M (2012) Oxide/water interfaces: how the surface chemistry modifies interfacial water properties. *Journal of Physics: Condensed Matter* 24(12):124106.
- 332 27. Bonthuis DJ, Netz RR (2013) Beyond the continuum: How molecular solvent structure affects electrostatics and hydrodynamics at solid-electrolyte interfaces. *Journal of Physical Chemistry B*
333 117(39):11397–11413.
- 334 28. Remsing RC, Weeks JD (2016) Role of Local Response in Ion Solvation: Born Theory and beyond. *Journal of Physical Chemistry B* 120(26):6238–6249.
- 335 29. Demille RC, Molinero V (2009) Coarse-grained ions without charges: Reproducing the solvation structure of NaCl in water using short-ranged potentials. *Journal of Chemical Physics* 131(3).
- 336 30. Wu Z, Cui Q, Yethiraj A (2010) A new coarse-grained model for water: The importance of electrostatic interactions. *Journal of Physical Chemistry B* 114(32):10524–10529.
- 337 31. Shin S, Willard AP (2018) Water's Interfacial Hydrogen Bonding Structure Reveals the Effective Strength of Surface–Water Interactions. *The Journal of Physical Chemistry B* 122(26):6781–6789.
- 338 32. Ósapay K, Young WS, Bashford D, Brooks CL, Case DA (1996) Dielectric continuum models for hydration effects on peptide conformational transitions. *Journal of Physical Chemistry* 100(7):2698–
339 2705.
- 340 33. Tamagawa H, Sakurai M, Inoue Y, Ariga K, Kunitake T (1997) Theoretical study of intermolecular interaction at the lipid-water interface. 2. Analysis based on the Poisson-Boltzmann equation.
341 *Journal of Physical Chemistry B* 101(24):4817–4825.
- 342 34. Koehl P, Orland H, Delarue M (2009) Beyond the Poisson-Boltzmann model: Modeling biomolecule-water and water-water interactions. *Physical Review Letters* 102(8):1–4.
- 343 35. Willard AP, Chandler D (2010) Instantaneous liquid interfaces. *The Journal of Physical Chemistry B* 114(5):1954–1958.
- 344 36. Shin S, Willard AP (2018) Three-Body Hydrogen Bond Defects Contribute Significantly to the Dielectric Properties of the Liquid Water-Vapor Interface. *Journal of Physical Chemistry Letters*
345 9(7):1649–1654.
- 346 37. Shiraga K, Ogawa Y, Kondo N (2016) Hydrogen Bond Network of Water around Protein Investigated with Terahertz and Infrared Spectroscopy. *Biophysical Journal* 111(12):2629–2641.
- 347 38. Bowman GR, Geissler PL (2012) Equilibrium fluctuations of a single folded protein reveal a multitude of potential cryptic allosteric sites. *Proceedings of the National Academy of Sciences of the*
348 *United States of America* 109(29):11681–11686.
- 349 39. Pezzella M, et al. (2020) Water dynamics around proteins: T- and r-states of hemoglobin and melittin. *Journal of Physical Chemistry B* 124(30):6540–6554.
- 350 40. Regmi R, et al. (2020) Phosphorylation-Dependent Conformations of the Disordered Carboxyl-Terminus Domain in the Epidermal Growth Factor Receptor. *Journal of Physical Chemistry Letters*
351 11(23):10037–10044.
- 352 41. Reichmann D, Phillip Y, Carmi A, Schreiber G (2008) On the contribution of water-mediated interactions to protein-complex stability. *Biochemistry* 47(3):1051–1060.
- 353 42. Plimpton S (1995) Fast Parallel Algorithms for Short-Range Molecular Dynamics. *Journal of Computational Physics* 117:1–19.
- 354 43. Berendsen HJC, Grigera JR, Straatsma TP (1987) The Missing Term in Effective Pair Potentials. *Journal of Physical Chemistry* 91(24):6269–6271.
- 355 44. Abraham FF, Singh Y (1977) The structure of a hard-sphere fluid in contact with a soft repulsive wall. *The Journal of Chemical Physics* 67(5):2384.
- 356 45. Lee C, McCammon JA, Rossky PJ (1984) The structure of liquid water at an extended hydrophobic surface. *The Journal of Chemical Physics* 80(9):4448–4455.
- 357 46. Yeh Ic, Berkowitz ML (1999) Ewald summation for systems with slab geometry. *Chemical Physics* 111(7):3155.
- 358 47. Ryckaert JP, Cicotti G, Berendsen HJ (1977) Numerical integration of the cartesian equations of motion of a system with constraints: molecular dynamics of n-alkanes. *Journal of Computational*
359 *Physics* 23(3):327–341.